Neurobiology of Aging 34 (2013) 1799–1806

Contents lists available at SciVerse ScienceDirect

Neurobiology of Aging

journal homepage: www.elsevier.com/locate/neuaging

Retinal ganglion cell dendritic degeneration in a mouse model of Alzheimer's disease

Pete A. Williams [a,1], Rebecca A. Thirgood [a], Huw Oliphant [b], Aura Frizzati [a], Elinor Littlewood [b], Marcela Votruba [a], Mark A. Good [c], Julie Williams [b], James E. Morgan [a,b,*]

[a] School of Optometry and Vision Sciences, Cardiff University, Cardiff, UK
[b] Cardiff University School of Medicine, Cardiff, UK
[c] School of Psychology, Cardiff University, Cardiff, UK

ARTICLE INFO

Article history:
Received 17 July 2012
Received in revised form 11 January 2013
Accepted 11 January 2013
Available online 7 March 2013

Keywords:
Retinal ganglion cell
Dendrite
Synapse
Alzheimer's disease
Mitochondrion
Hippocampus

ABSTRACT

Retinal ganglion cells (RGCs) may be regarded as a target biomarker in Alzheimer's disease (AD). We therefore explored the possibility that RGC degeneration, rather than cell loss, is an early marker of neuronal degeneration in a murine model of AD. RGC dendritic morphology and dendritic spine densities of CA1 hippocampal pyramidal neurons were quantified in 14-month-old transgenic mice expressing the APP(SWE) (amyloid precusor protein-Swedish mutation) mutation (Tg2576). The dendritic integrity of RGCs was found to be significantly reduced in the absence of significant RGC loss in Tg2576 mice compared with age-matched wild-type controls. In hippocampal CA1 pyramidal neurons, we observed dendritic spines to be present at a lower frequency from the same animals, but this did not reach significance. Synaptic and mitochondrial protein expression markers (PSD95 [postsynaptic density protein 95], synaptophysin, and Mfn2 [mitofusin 2]) showed no significant changes in RGC synaptic densities but a highly significant change in mitochondrial morphology with a marked reduction in the integrity of the mitochondrial cristae. Our findings suggest that, in a well-characterized mouse model of AD, RGC dendritic atrophy precedes cell loss, and this change may be because of accumulations of amyloid-β. Because RGC dendrites are confined to the inner plexiform layer of the retina, imaging techniques that focus on this layer, rather than the loss of RGCs, may provide a sensitive biomarker for monitoring neural damage in AD.

1. Introduction

Alzheimer's disease (AD) remains a major cause of cognitive decline in the Western population. Considerable advances have been made in our understanding of the genetic basis of this disease, but the development of biomarkers for staging the disease remains a challenge. In the search for an optimal set of biomarkers, central nervous system imaging has shown the most promise (McEvoy and Brewer, 2010) and significant progress has been made in the use of magnetic resonance imaging in combination with ligands that can highlight areas of central nervous system pathology (Rowe et al., 2007, 2008) and positron emission tomography (Klunk et al., 2004) (reviewed in Furst and Kerchner, 2012). These methods rely either on the detection of amyloid plaques or on the neuronal and axonal loss. Although these are important stages in the disease process, there is compelling evidence that neurons undergo a prolonged period of degeneration before cell death, manifest as neurite loss and dendritic pruning (Anderton et al., 1998; Selkoe, 2002). The hippocampus and entorhinal cortex have consistently demonstrated early neuronal damage in AD, but the detection of this neurite loss in vivo in these areas is problematic.

The retina is the only tissue in which neurons can be imaged on a repeatable and long-term basis; the eye has, therefore, been considered as a "window on the brain" where optical imaging might enhance our ability to detect neurodegenerative disease (Koronyo et al., 2012; Koronyo-Hamaoui et al., 2011; Miller and Drachman, 2006). Recent developments in interference-based imaging methods, such as optical coherence tomography (OCT), indicate that it is possible to detect optical signals arising from changes in subcellular structures (Gossage et al., 2003; Kajic et al., 2010). Ultra–high-resolution OCT can provide retinal images at resolutions that are subcellular without the need for exogenous ligands (Drexler and Fujimoto, 2008; Povazay et al., 2009) raising the prospect that these imaging technologies could be used clinically to characterize retinal neuronal changes. Retinal ganglion cells (RGCs) in particular comprise an ideal candidate population

* Corresponding author at: School of Optometry and Vision Sciences, Cardiff University, Maindy Road, Cardiff CF24 4LU, UK. Tel.: +44 29 20876344.
E-mail address: morganje3@cardiff.ac.uk (J.E. Morgan).
[1] Present address: The Jackson Laboratory, 600 Main Street, Bar Harbor, ME 04609, USA.

0197-4580/$ – see front matter © 2013 Elsevier Inc. All rights reserved.
http://dx.doi.org/10.1016/j.neurobiolaging.2013.01.006

(Cordeiro et al., 2010). They may be uniquely vulnerable to the effects of neurodegeneration because they have long axons for which the intraocular portion is unmyelinated thereby increasing energy requirements and cellular stress. Several investigators have tested the possibility that this cell population may be reduced in AD (Jindahra et al., 2010). In addition, amyloid-β (Aβ) deposits, a hallmark feature of AD, have been found in both AD patients and animal models of AD (Koronyo-Hamaoui et al., 2011). Postmortem studies in patients with AD have, however, been equivocal with regard to the loss of RGCs; some have reported significant reductions in RGC populations (Blanks et al., 1989, 1996b), but these have not been confirmed by others (Curcio and Drucker, 1993). Clinical imaging studies using OCT have reported significant loss of cells in the RGC layer with corresponding thinning of the retinal nerve fiber layer in patients with clinically manifest AD (Paquet et al., 2007). The development of novel ligands to identify in vivo RGC death driven by the experimental administration of Aβ peptide (1–40) raises the possibility that RGC loss could provide a valuable biomarker for AD (Guo et al., 2007).

Because a loss of synaptic connectivity is likely to be one of the earliest pathological changes in AD rather than neuronal loss (Selkoe, 2002), we reasoned that RGC dendritic integrity would provide a sensitive marker of neuronal degeneration. Reduced dendrite complexity has been reported in models of chronic RGC degeneration (Morgan et al., 2006; Weber et al., 1998; Williams et al., 2012). Because these changes are similar to those observed in AD (Scheff and Price, 2003; Scheff et al., 2006; Selkoe, 2002), we tested the hypothesis that RGC dendritic degeneration may provide a marker for central nervous system damage in a mouse (Tg2576) model of amyloid pathology. Animals were evaluated at 14 months of age by which time they have developed significant cognitive deficits associated with the deposition of Aβ plaques in cortical and limbic structures (Hsiao et al., 1996).

2. Materials and methods

2.1. Retinal preparation

All animals were in good health at the time of the study. Fourteen-month-old, female APP(SWE) Tg2576 mice (Tg, $n = 9$) (Chapman et al., 1999) and their age- and sex-matched control littermates (WT, $n = 8$) were killed by cervical dislocation, and the eyes were quickly enucleated and placed in chilled (4 °C) HBSS (Hank's balanced salt solution) (Invitrogen, UK). The eyes were punctured at the limbus and a slit cut in the sclera to remove the cornea and sclera anterior to the ora serrata, along with the lens and vitreous. Three cuts were made in the retina before it was flat-mounted, ganglion cell layer up, on a cell culture insert (Millipore, Billerica, MA, USA) and submerged in custom media (CM) containing Neurobasal media, 2% B-2 supplement, 1% N-27 supplement, and 0.5 mM glutamate (Invitrogen). Retinas were incubated at 37 °C and 4% CO_2 ready for DiOlistic labeling using a gene gun or labeling with Hoechst 33258 stain. The total time between death and DiOlistic labeling was less than 10 minutes. Because the APP(SWE) Tg2576 transgenic mouse line carries the retinal degeneration, "*rd*," mutation that adversely affect retinal anatomy, all mice were routinely genotyped to exclude any $rd^{-/-}$ mice from the study.

2.2. Brain slice preparation

The brains from all mice were sectioned sagittally in an ice-cold phosphate-buffered saline (PBS) at 250 μm using a Leica VT1000S vibratome (Leica Microsystems, UK). Approximately 3 consecutive sections from each brain hemisphere were immediately placed into CM in 6-well plates. The CM was then removed for DiOlistic labeling, replaced, and incubated at 37 °C and 4% CO_2. The total time between death and DiOlistic labeling of brain slices was less than 25 minutes.

2.3. DiOlistic labeling

DiOlistics, a modified gene-gun procedure, which has been previously used to quantify dendritic changes in AD models (Smith et al., 2009), relies on the affinity of carbocyanine dyes to the phospholipid membrane of cells. Using a relatively high pressure (typically greater than 100 psi), carbocyanine dyes adhered to tungsten particles are propelled through the barrel of the gene-gun into the tissue in culture (O'Brien and Lummis, 2004, 2006). This method gives 2 main advantages over common immunohistochemical (IHC) labeling or tracer studies: (1) labeling is random and typically with a low yield allowing for individual cells to be morphometrically analyzed; and (2) these dyes distribute along the membrane regardless of the cell's physiological status.

The setting for bead delivery and preparation for DiOlistic labeling has been described in detail elsewhere (Gan et al., 2000; Sun et al., 2002). Briefly, 100 mg of tungsten particles (1.7 μm; Bio-Rad, Hercules, CA, USA) was placed in a thin, even layer on a clean, glass slide. DiI (1,1′-dioctadecyl-3,3,3′3′-tetramethylindocarbocyanine perchlorate) (80 μg; Invitrogen) was then mixed in 800 μL of methylene chloride and poured over the tungsten particles. The methylene chloride evaporated quickly to leave DiI-coated tungsten particles, which were then transferred onto clean wax-paper or tinfoil. This powder was then funneled into a length of 1.4 mm "Gold-Coat" tubing (Bio-Rad) and allowed to settle, resulting in a light application of the powder on the inside of the tubing. Excess powder was funneled off, and the tubing was cut into 1.2 cm lengths for storage in the dark at room temperature (RT) ready for use.

Retinas were shot once at 100 psi using a Helios gene gun (Bio-Rad) through a 3.0-μm pore size, high pore density, cell culture insert (Becton Dickinson, Franklin Lakes, NJ, USA) to block the passage of aggregated tungsten particles. The barrel of the gun was held 5 cm above the retinal explant. Retinas were then incubated for 30 minutes to facilitate dye diffusion before being placed in 4% PFA at RT for a further 30 minutes. Retinal preparations were then mounted RGC side up and coverslipped under ProLong Gold AntiFade Reagent (Invitrogen) containing 1 μg/mL Hoechst 33258 as a nuclear counterstain and sealed with nail polish. Hippocampal slices were shot at 150 psi from 5 cm with a 3.0-μm pore size cell culture insert before being incubated for 30 minutes to facilitate dye diffusion before being placed in 4% PFA at RT for a further 30 minutes. The slices were then mounted in ProLong Gold Anti-Fade Reagent and sealed with nail polish. Images were taken within 24 hours from both retinal and brain samples.

2.4. RGC dendrite morphological analysis

Image stacks of 142 RGCs (0.5 μm slice width) were obtained with a Zeiss LSM 510 confocal microscope (Carl Zeiss Ltd, UK) using a 20× objective to allow the capture of the entire dendritic tree in a single image. Dendritic morphologies were analyzed using ImageJ to measure dendritic field area (measured using the convex polygon tool to join the outermost points of the dendritic tree), an ImageJ plugin, NeuronJ to measure total dendritic length, and a custom Matlab macro to run a Sholl analysis (Gutierrez and Davies, 2007).

2.5. Ganglion cell layer cell counts

For RGC counts, the methods outlined by Jakobs et al. (2005) were used with minor modifications. All retinas were stained with Hoechst 33258 to allow for ganglion cell layer cell counts.

Images were taken from the RGC layer at 2 retinal locations, 1 mm superior and inferior to the optic disc using a Leica DM6000 B confocal microscope (Leica Microsystems) with a 20× objective. Cells were manually counted in a 300-μm^2 area using the ImageJ counter plugin.

2.6. Dendritic spine analysis

Image stacks of entire dendrites of pyramidal neurons with somas inside the CA1 field of the hippocampus were collected using a Zeiss LSM 510 confocal microscope (Carl Zeiss Ltd) captured at a 40× oil-immersion objective allowing the whole dendrite to be shown and with clear contrast of dendritic spines. Dendrites were measured using ImageJ, and spine counts were taken manually using the ImageJ counter plugin. Spine counts were expressed as a dendritic spine density (spines per 1 μm dendrite).

2.7. IHC labeling of retinal sections and retinal thickness

Adult (12-month-old), female Tg mice ($n = 17$) and their age- and sex-matched control littermates (WT, $n = 14$) were PBS perfused before being cervically dislocated, and the eyes were quickly enucleated, punctured at the limbus, and then submerged in 4% paraformaldehyde (PFA) at 4 °C for 30 minutes. Eyes were washed (1% PBS) and placed in a 30% sucrose solution in PBS at 4 °C for 24 hours. Eyes were then frozen in OCT compound (Sakura Finetek, UK) and cut at 20 μm using a cryostat at −23 °C. For IHC staining, the techniques outlined in the literature (Chetkovich et al., 2002) were followed with minor alterations. Briefly, slide-mounted sections were warmed to RT for 30 minutes and then permeabilized with 0.2% Tween (PBST). Sections were blocked with 5% chick serum in PBS at RT for 1 hour and incubated with goat anti-PSD95 (polyclonal, 1:400, #AB12093; Abcam, UK), rabbit anti-synaptophysin (polyclonal, 1:250, #AB14692; Abcam), rabbit anti-γ-synuclein (monoclonal, 1:200, #AB55424; Abcam), rabbit anti-mitofusin 2 (polyclonal, 1:200, #AB50843; Abcam), or rabbit anti-Aβ 1–42 (polyclonal, 1:100, #AB10148; Abcam) in 5% chick serum in PBS at 4 °C overnight. Sections were washed 3 times for 2 minutes in PBST and incubated with chicken anti-rabbit AF488-conjugated antibody (1:500) and TO-PRO-3-Iodide (1:500) (Invitrogen) at RT for 2 hours. They were then washed 3 times for 2 minutes in PBST, mounted in ProLong Gold AntiFade Reagent, coverslipped, and sealed with nail varnish. Z-stack images were taken with 96 hours of mounting using a Zeiss LSM 510 laser scanning confocal microscope at 20× and processed using ImageJ. For RGC counts, the "cell counter" plugin was used, and cell populations are expressed as a percentage change from WT. For quantification of antibody markers, image stacks were z-projected, the color channel with the secondary fluorophore was cropped out, and the pixel density was measured. For retinal layer thickness width of each individual, retinal layer was measured using ImageJ's Measure tool. For each retina, 10–20 sections were used for analysis.

2.8. Electron microscopy

Adult (12-month-old), female Tg mice ($n = 4$) and their age- and sex-matched control littermates (WT, $n = 4$) were PBS perfused before being cervically dislocated, eyes quickly removed, and their whole retinas fixed in 1% glutaraldehyde in Sorensen's PB. Retinas were postfixed in 1% osmium tetroxide for 2 hours, thoroughly washed, and dehydrated through graded ethanol (50%, 70%, 90%, and 100% for 15 minutes each) followed by 3 exchanges of propylene oxide for 10 minutes each. Retinas were then infiltrated for 45 minutes in 50% TAAB embedding resin (TER) (TAAB Laboratories Equipment Ltd, UK) in propylene oxide, followed by 3 × 1 hour in 100% TER before being embedded in 100% TER at 60 °C for 48 hours. Eighty-nanometer-thick sections were collected onto 300 mesh copper grids, stained for 30 minutes in saturated uranyl acetate, washed, and stained again using Reynolds lead citrate (Reynolds, 1963) for 15 minutes before being air dried. Samples were examined in a Philips CM12 TEM (FEI UK Ltd, UK) at 80 kV. Mitochondrial images from RGC dendrites in the inner plexiform layer were captured with a Megaview III camera and AnalySIS software (Soft Imaging System GmbH, Germany). A mitochondria complexity index was calculated by summing the number of intersections of mitochondrial cristae falling on a line running along (1) minor; and (2) major mitochondrial axes for imaged mitochondria ($n = 100$) (Fig. 1). The number of intersections is expressed as a mean value per mitochondrion.

Statistical analyses were performed using SPSS software (version 16.0.2; SPSS, Chicago, IL, USA) and Microsoft Excel (Microsoft, Redmond, WA, USA). All analyses were masked to disease status.

3. Results

3.1. DiOlistic labeling of RGCs and CA1 region pyramidal neurons

The analysis of RGC dendritic morphology is based on 72 cells from 8 WT mice and 70 cells from 9, 14-month-old Tg mice. Typical DiOlistically labeled cells are shown in Fig. 2 with examples of RGCs from WT mice in Fig. 2A and B. The Tg animals showed a range of changes with a combination of cells with minimal or no damage (Fig. 2D) to those with marked dendritic atrophy (Fig. 2E). For inclusion in the analysis, RGCs were identified by the presence of an axon projecting to the optic disc. Any cells lacking an axon, even though they might possess somal and dendritic characteristics typical of RGCs, were excluded from the analysis. There are as many as 14 different types or morphologies for RGCs within the mouse retina based on their dendritic architecture (Coombs et al., 2006; Doi et al., 1995; Kong et al., 2005; Sun et al., 2002). It is important to classify cells from the control eyes to account for any potential bias during the investigation (although this cannot be done on the Tg RGCs as their dendritic architectures may be already compromised).

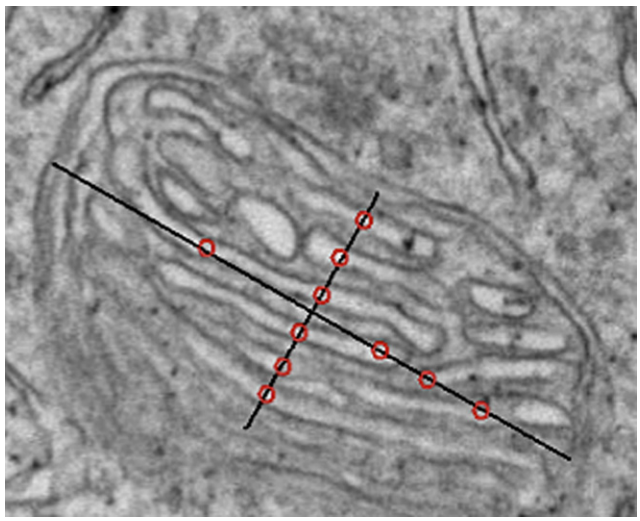

Fig. 1. Mitochondrial complexity index (MCI). The MCI was calculated by counting the number of intersections (represented as red circles) of mitochondrial cristae along both the major (longest length of the mitochondria) and the minor (width) axes (black lines). Mitochondrion shown is from a WT mouse.

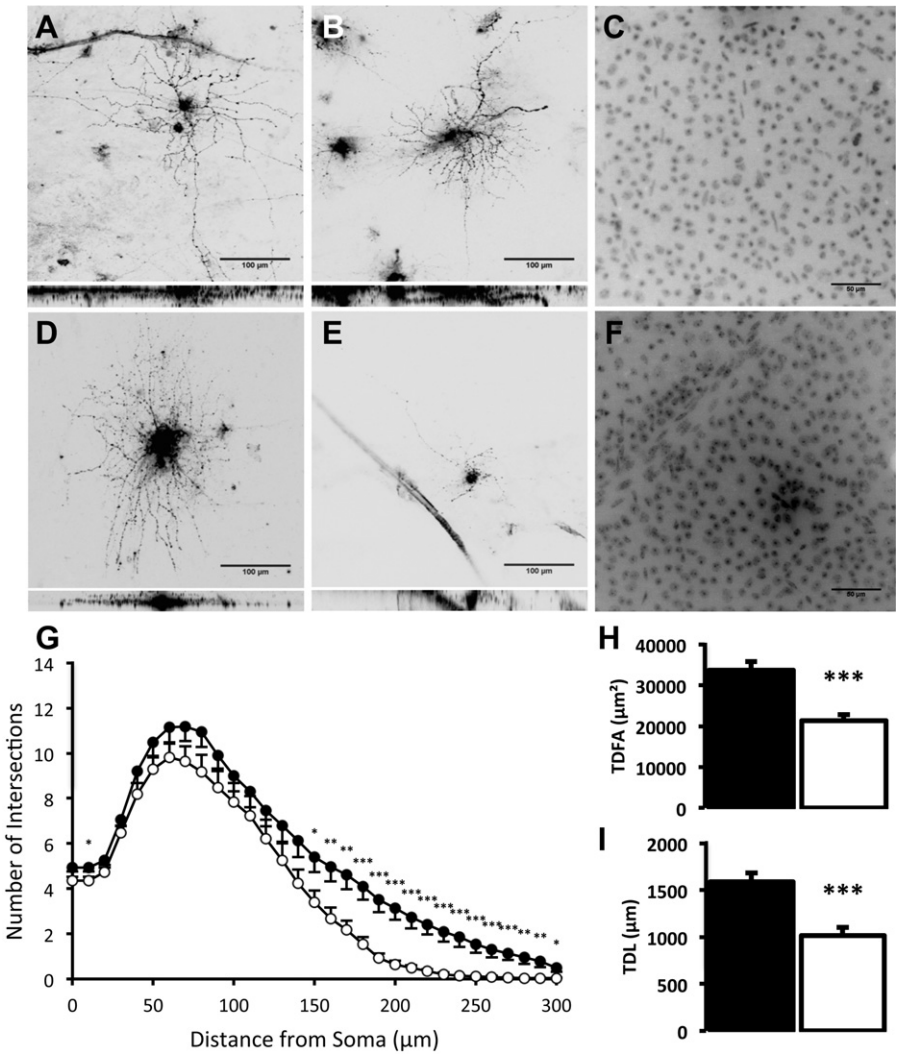

Fig. 2. Retinal ganglion cell (RGC) dendritic integrity is reduced in Tg mice in the absence of soma loss. (A–F) Compressed confocal stacks of DiOlistically labeled WT (A, B) and Tg (D, E) RGCs with representative Hoechst-labeled cell bodies (C, WT; F, Tg). En face view (xy plane) (top) and side-on view (xz plane) (bottom). All scale bars = 100 μm. (G) Sholl analyses of WT (black circles) and Tg (white circles) RGC dendritic integrity are reduced in Tg RGCs as shown by the down- and leftward shifts in the Sholl plot (area under the curve $p < 0.0001$). (H–I) Total dendritic field area (TDFA) (H) and total dendritic length (TDL) (I) are reduced in Tg (white) RGCs compared with age- and sex-matched WT controls (black) (−34.4% TDFA, −32.4% TDL). Error bars = standard error of the mean, $^{*}p < 0.05$, $^{**}p < 0.01$, and $^{***}p < 0.0001$.

The use of IHC markers for differing cell types combined with DiOlistics was excluded because cell permeabilization disrupted the cell membrane and compromised the quality of DiOlistic labeling. Therefore, only cells from the control eyes were classified according to the criteria of Sun et al. (2002) (RGC types [% sampled/% expected]; A1 [10%/10%], A2 [5%/13%], B2 [26%/21%], B3 [30%/24%], B4 [8%/13%], C3 [15%/5%], and C4 [6%14%]).

The distribution of dendritic complexity as a function of distance from the cell soma is shown in Fig. 2G. The Sholl plot confirmed a significant reduction in dendritic complexity from mid to peripheral parts of the dendritic tree. We observed a significant, 34.4% reduction in dendritic field area (±standard error of the mean [SEM]) (WT, 33,680 ± 2034 μm^2; Tg, 22,083 ± 1573 μm^2; $p < 0.0001$) for RGCs from Tg animals, as shown in Fig. 2. Consistent with this, total dendritic length was reduced by 32.4% in Tg animals (±SEM) (WT, 1589 ± 95 μm; Tg, 1074 ± 99 μm; $p < 0.0001$). RGC counts, estimated from total cell counts in the RGC layer (Jakobs et al., 2005), were not significantly reduced in retinas from Tg mice (WT, 469.1 cells/300 μm^2; Tg, 446.5 cells/300 μm^2; reduction, 5%; $p > 0.05$, Fig. 2C and F). In addition, there was no change in the thickness of ganglion cell layer (WT, 10.4 ± 0.5 μm; Tg, 12.3 ± 0.6 μm; $p > 0.05$) or inner plexiform retinal layer (WT, 49.6 ± 2.1 μm; Tg, 50.6 ± 2.7 μm; $p > 0.05$).

The same animals providing cells for the retinal analysis were used to quantify the number of dendritic spines of dendrites in the CA1 pyramidal field of the hippocampus. Fig. 3 shows DiOlistically labeled dendrites in the hippocampal CA1 field from WT and Tg mice. Subjectively, we did not observe a marked difference in spine density between the 2 strains. In a quantitative analysis, we counted 2613 spines from 124 dendrites in Tg animals and 3958 spines from 185 dendrites in WT animals (Fig. 3E). Although we observed a general reduction in the number of spines in the TG animals, this did not reach conventional levels of significance (spines/μm ± SEM; WT, 0.2679 ± 0.086; Tg, 0.2490 ± 0.076; reduction, 7.1%; $p = 0.05070$).

3.2. RGC synaptic and mitochondrial analysis

IHC was used to explore the molecular changes underlying RGC dendritic pruning. Antibodies to probe amyloid pathology in the

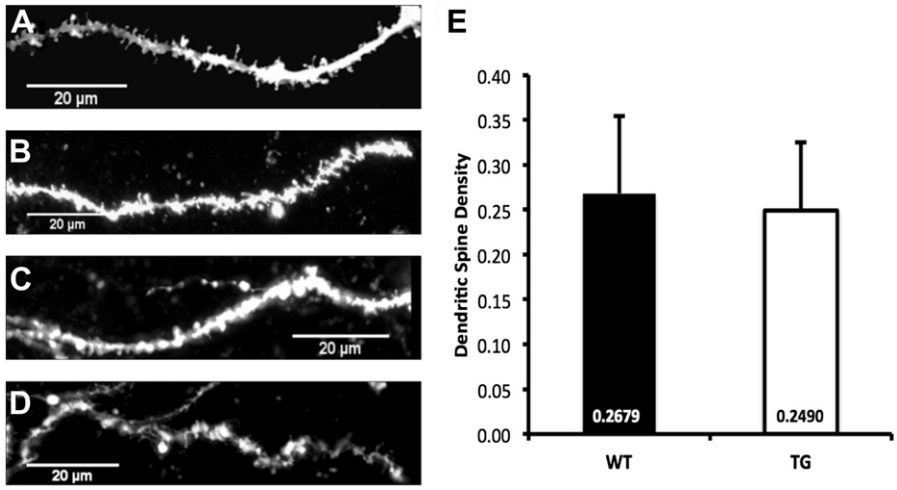

Fig. 3. Synaptic density is not significantly reduced in WT and Tg CA1 pyramidal neurons. (A, B) Representative dendrites CA1 region of the hippocampus in WT mice, DiOlistically labeled. (C, D) Representative dendrites from Tg mice. All scale bars = 20 μm. (E) Spine density measurements (standard error of the mean) for WT (black) and Tg (white) (C, D) mice ($p > 0.05$).

retina (Aβ42, Fig. 4A–C) showed light labeling for Aβ42 in the RGC and inner plexiform layers of both Tg and WT animals with lighter labeling in the outer plexifom layer. Quantitative analysis of labeling in the RGC or inner plexiform layers showed that this was significantly elevated in the Tg animals (percentage change from WT ± SEM; WT, 100.0 ± 3.4; Tg, 112.6 ± 5.1; $p < 0.05$). PSD95 was used as a marker of postsynaptic and synaptophysin of presynaptic integrity as shown in Fig. 4D–F and Fig. 4G–I, respectively. We did not see a change in the density of the synaptic proteins: PSD95 (WT, 100.0 ± 4.8; Tg, 110.3 ± 5.7; $p > 0.05$) and synaptophysin (WT, 100.0 ± 5.5; Tg, 109.6 ± 6.7; $p > 0.05$). Mfn2 labeling (Fig. 4J–L) was used as a marker for the distribution of mitochondria that did not show a significant difference in WT and Tg strains (WT, 100.0 ± 3.9; Tg, 103.6 ± 4.2; $p > 0.05$). However, electron microscopic analysis of mitochondrial structure showed a significant decrease in mitochondrial complexity in the Tg animals (mitochondrial complexity index, mean number of mitochondrial cristae intersected ± SEM; WT, 2.97 ± 0.31; Tg, 0.97 ± 0.22; $p < 0.001$). We also observed mitochondrial swelling throughout RGC dendrites in Tg animals with large intermitochondrial spaces and fragmented cristae (Fig. 5).

4. Discussion

We show, for the first time, evidence of RGC dendritic pruning in a murine model of AD-related amyloid pathology. These degenerative changes may precede, or at least accompany, any deterioration in synaptic spine density in the hippocampus. However, it is interesting to note that we did not observe a reduction in synaptic density that correlated with the reduction in dendritic complexity. This may be, in part, because of the moderate shrinkage of the dendritic field that preserved the synaptic number and, therefore, synaptic density.

The retina has been used by a number of groups as a potential substrate for clinical staging of AD, but the focus has hitherto been on RGC loss, for which a consistent histologic outcome has not been reported, and which may occur relatively late in the course of the disease. Curcio and Drucker (1993) reported the absence of AD-specific RGC loss. By contrast, others have reported up to 47% cell loss in the parafoveal RGC layer (Blanks et al., 1996a, 1996b) in eyes from AD patients. These discrepancies may have arisen from the use of different histologic methods and criteria for RGC identification (Curcio and Drucker, 1993) and the analysis of patients at differing stages of AD.

APP is synthesized in healthy RGCs (Morin et al., 1993), and the retinal deposition of APP has been reported in Tg mice with robust labeling in the RGC and inner nuclear layer (Dutescu et al., 2009), but without Aβ plaque formation. Moderate increases in terminal deoxynucleotidyl transferase dUTP nick end labeling (TUNEL)-positive RGCs have been noted in mice harboring the Tg and presenilin mutations (Ning et al., 2008) associated with Aβ in the RGC layer (Koronyo-Hamaoui et al., 2011; McKinnon et al., 2002). In the APP(SWE) or PS1E9 transgenic mouse, these changes were associated with compromised retinal function as measured by electroretinography (Perez et al., 2009) in the absence of significant neuronal loss.

Aβ is also deposited in the outer retinal layers as part of the aging process where it may be associated with degeneration at the photoreceptor layer (Lee et al., 2012; Ning et al., 2008). In aged human retinas, Aβ deposition has been reported in drusen that can underlie the onset of age-related macular degeneration (Ohno-Matsui, 2011). The extent to which outer retinal degeneration drives inner retinal neuritic changes is unclear. A recent report that outer retinal degeneration can drive RGC dendritic atrophy as a result of transneuronal changes in mice may provide an explanation for some of the changes seen in our animals (Damiani et al., 2012). We observed preservation of the retinal laminar architecture in contrast to the previous reports from 14-month-old Tg2576 mice (Liu et al., 2009). The difference may reflect accelerated neuronal loss and retinal inflammation that is not apparent at 12 months.

Although these transgenic models have provided valuable insights into the effects of Aβ deposition on retinal structure and function, they should be interpreted with caution because of the possibility of other genetic defects with inbred strains. Thus, C57B6 can carry an *rd* mutation affecting the rod-specific cGMP-PDE gene resulting in outer retinal (photoreceptor) degeneration by P25 (Jimenez et al., 1996). These mutations can be an important potential confounder in the assessment of these mice for the functional impact of amyloid deposition (Garcia et al., 2004).

The mechanisms by which Aβ deposition results in dendritic pruning remains unclear but of great importance given the role of synaptic loss as a fundamental pathological mechanism in AD (Selkoe, 2002). One possibility is that intraneuronal Aβ deposition may compromise mitochondrial structure and initiate synaptic

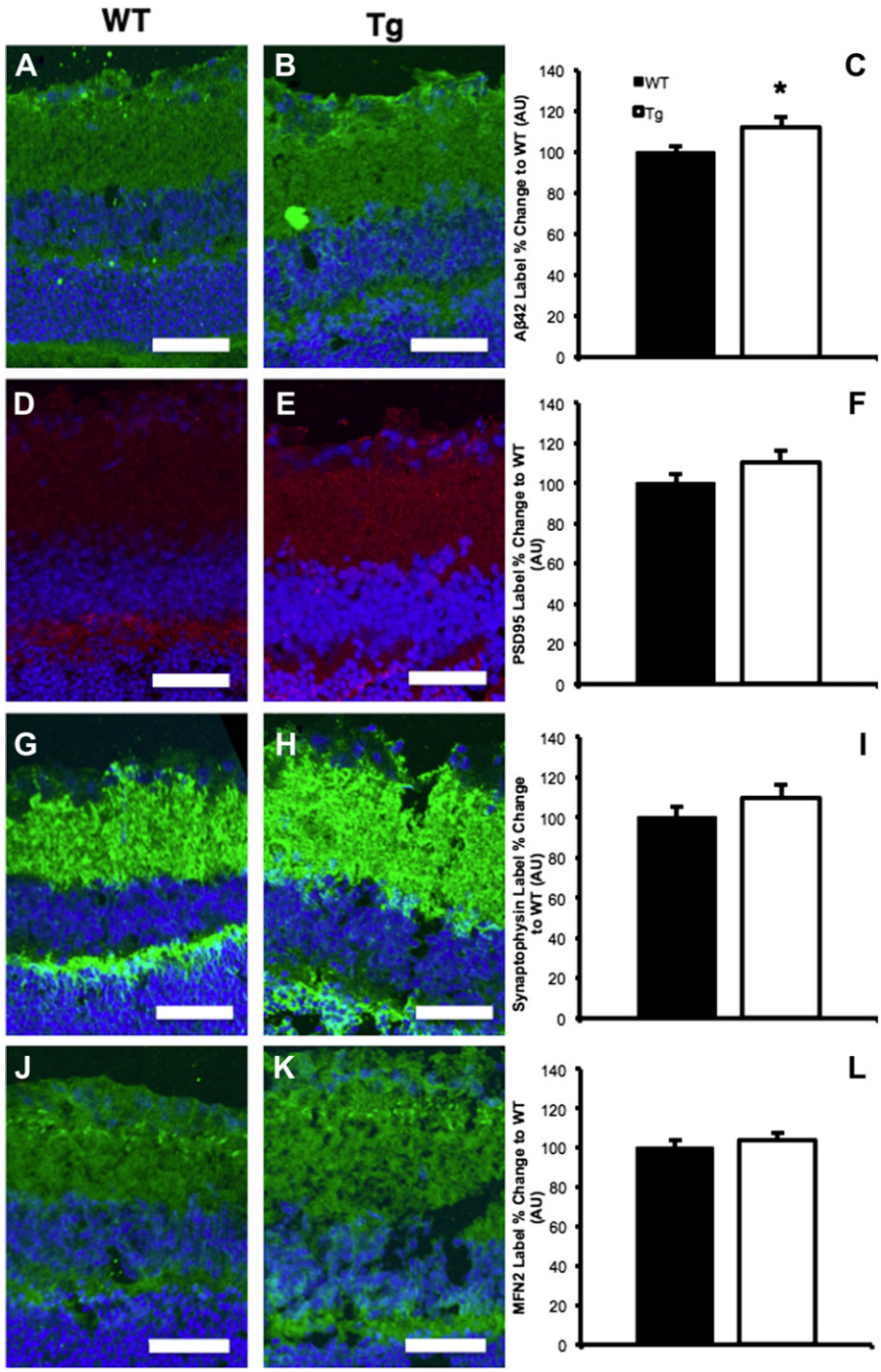

Fig. 4. No change in synaptic or mitochondrial density in the inner plexiform layer of Tg mice. (A, B) Representative samples of WT (A) and Tg (B) mouse retina stained for Aβ42, and there is a significant increase in Aβ42 immunoreactivity in the Tg retina (C). (D, E) Representative samples of WT (D) and Tg (E) mouse retina stained for PSD95, and there was no significant change in synaptic densities as measured by PSD95 between WT and Tg mouse retina (F). (G, H) Representative samples of WT (G) and Tg (H) mouse retina stained for synaptophysin, and there was no significant change in synaptic densities as measured by synaptophysin between WT and Tg mouse retina (I). Mfn2 was used as a marker of mitochondria (J, WT; K, Tg). There was no significant change in mitochondrial densities between WT and Tg mouse retina (L). Scale bars = 50 μm. Error bars = standard error of the mean. $^{*}p < 0.05$ (Student t test).

depletion in the dendritic tree (Calkins et al., 2011). RGCs may be particularly vulnerable to this effect because RGC axons only myelinate when they enter the optic nerve and, therefore, rely on energy intensive non-saltatory propagation in the intraretinal compartment (Osborne, 2008). These demands are reflected in the large numbers of mitochondria within the dendritic and axonal compartments (Wang et al., 2003). Defective mitochondrial function can generate a similar RGC phenotype to that seen in AD. For example, in Opa1 mutant mice, RGC dendritic atrophy occurs in the absence of significant levels of RGC death (Williams et al., 2010, 2012). It is interesting to note that the levels of mitochondrial shaping proteins (Opa1, Dnm1, Mfn1, and Mfn2) are reduced in AD (Wang et al., 2008, 2009) and that increased mitochondrial fission and reduced fusion have been reported in human AD (Manczak et al., 2011). Furthermore,

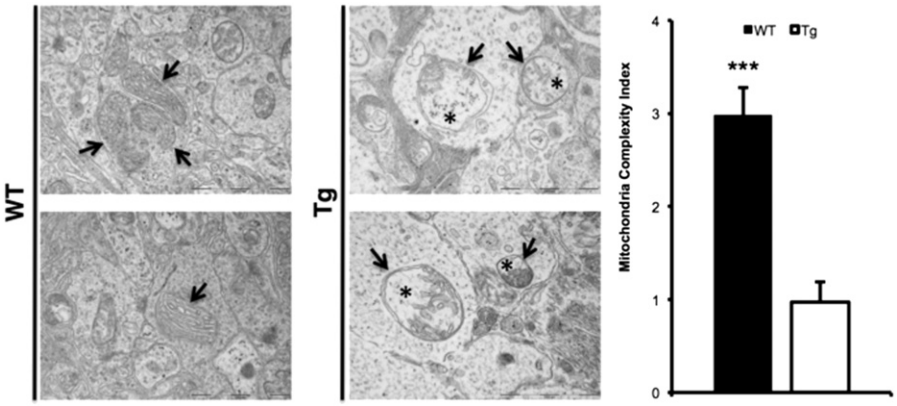

Fig. 5. Mitochondrial integrity is significantly reduced in Tg retinal ganglion cells (RGCs). Representative electron micrographs of WT and Tg RGC mitochondria (black arrows). There is a significant decrease (Tg, 67.3%; $p < 0.001$) in the mitochondria complexity index (lower graph) in Tg RGC mitochondria. Tg RGC dendrites show aberrant mitochondria with visibly absent cristae resulting in considerable intermitochondrial space (asterisks). Scale bar = 2 μm. Error bars = standard error of the mean. $^{***}p < 0.001$ (Student *t* test).

RGCs are exposed to light, which may increase the potential for mitochondrial dysfunction and render RGC mitochondria particularly vulnerable to the effects of APP deposition (Osborne et al., 2006).

Extra neuronal factors may also contribute to dendritic remodeling. APP can induce an inflammatory response manifest by the infiltration of microglia (Liu et al., 2009) similar to that seen in glaucoma in association with dendritic pruning (Yu et al., 2012). Microglia have been shown to be important in mediating RGC degeneration in other diseases (Naskar et al., 2002) raising the possibility that they could be used a marker of early damage in experimental AD because they can be imaged, in vivo, in the murine retina (Liu et al., 2012).

What are the implications of our findings for clinical practice and the development of biomarkers for AD? If similar RGC degenerative changes occur in the human retina, then imaging the synaptic layer of the RGC, the inner plexiform layer, may be a useful marker (in combination with other diagnostic tools) for the early detection of AD-related neurodegeneration. Clinical studies have shown thinning of the retinal nerve fiber layer, which would be consistent with the loss of RGCs, although this was noted only in patients with manifest disease (Lu et al., 2010). Our data suggest that dendritic changes precede cell loss and are, therefore, likely to occur in patients with early AD, which would be a significant diagnostic advance. Considerable progress has been made in the development of retinal imaging modalities (e.g., ultra–high-resolution OCT) that allow delineation of the various layers of the retina at near cellular resolutions (Torti et al., 2009). The refinement of these techniques for the detection of degeneration within the inner retinal synaptic layer is likely to be of significant clinical benefit.

Disclosure statement

None of the authors has a financial declaration to make relevant to the submitted work.

The animal work was conducted in accordance with Home Office (UK) regulations on the use of animals in research.

Acknowledgements

We gratefully acknowledge Ms Elaine Taylor for the polymerase chain reaction screening of *rd* mutants and Ms Alice Palmer for providing the mice. The work was funded by Medical Research Council (J.W.), Wellcome Trust (M.G.), and Alzheimer's Trust (M.G.).

References

Anderton, B.H., Callahan, L., Coleman, P., Davies, P., Flood, D., Jicha, G.A., Ohm, T., Weaver, C., 1998. Dendritic changes in Alzheimer's disease and factors that may underlie these changes. Prog. Neurobiol. 55, 595–609.

Blanks, J.C., Hinton, D.R., Sadun, A.A., Miller, C.A., 1989. Retinal ganglion cell degeneration in Alzheimer's disease. Brain Res. 501, 364–372.

Blanks, J.C., Schmidt, S.Y., Torigoe, Y., Porrello, K.V., Hinton, D.R., Blanks, R.H., 1996a. Retinal pathology in Alzheimer's disease. II. Regional neuron loss and glial changes in GCL. Neurobiol. Aging 17, 385–395.

Blanks, J.C., Torigoe, Y., Hinton, D.R., Blanks, R.H., 1996b. Retinal pathology in Alzheimer's disease. I. Ganglion cell loss in foveal/parafoveal retina. Neurobiol. Aging 17, 377–384.

Calkins, M.J., Manczak, M., Mao, P., Shirendeb, U., Reddy, P.H., 2011. Impaired mitochondrial biogenesis, defective axonal transport of mitochondria. Hum. Mol. Genet. 20, 4515–4529.

Chapman, P.F., White, G.L., Jones, M.W., Cooper-Blacketer, D., Marshall, V.J., Irizarry, M., Younkin, L., Good, M.A., Bliss, T.V., Hyman, B.T., Younkin, S.G., Hsiao, K.K., 1999. Impaired synaptic plasticity and learning in aged amyloid precursor protein transgenic mice. Nat. Neurosci. 2, 271–276.

Chetkovich, D.M., Bunn, R.C., Kuo, S.-H., Kawasaki, Y., Kohwi, M., Bredt, D.S., 2002. Postsynaptic targeting of alternative postsynaptic density-95 isoforms by distinct mechanisms. J. Neurosci. 22, 6415–6425.

Coombs, J., van der List, D., Wang, G.Y., Chalupa, L.M., 2006. Morphological properties of mouse retinal ganglion cells. Neuroscience 140, 123–136.

Cordeiro, M.F., Guo, L., Coxon, K.M., Duggan, J., Nizari, S., Normando, E.M., Sensi, S.L., Sillito, A.M., Fitzke, F.W., Salt, T.E., Moss, S.E., 2010. Imaging multiple phases of neurodegeneration: a novel approach to assessing cell. Cell Death Dis. 1, e3.

Curcio, C.A., Drucker, D.N., 1993. Retinal ganglion cells in Alzheimer's disease and aging. Ann. Neurol. 33, 248–257.

Damiani, D., Novelli, E., Mazzoni, F., Strettoi, E., 2012. Undersized dendritic arborizations in retinal ganglion cells of the rd1 mutant. J. Comp. Neurol. 520, 1406–1423.

Doi, M., Uji, Y., Yamamura, H., 1995. Morphological classification of retinal ganglion-cells in mice. J. Comp. Neurol. 356, 368–386.

Drexler, W., Fujimoto, J.G., 2008. State-of-the-art retinal optical coherence tomography. Prog. Retin. Eye Res. 27, 45–88.

Dutescu, R.M., Li, Q.X., Crowston, J., Masters, C.L., Baird, P.N., Culvenor, J.G., 2009. Amyloid precursor protein processing and retinal pathology in mouse models of Alzheimer's disease. Graefes. Arch. Clin. Exp. Ophthalmol. 247, 1213–1221.

Furst, A.J., Kerchner, G.A., 2012. From Alois to Amyvid: seeing Alzheimer disease. Neurology 79, 1628–1629.

Gan, W.B., Grutzendler, J., Wong, W.T., Wong, R.O., Lichtman, J.W., 2000. Multicolor "DiOlistic" labeling of the nervous system using lipophilic dye combinations. Neuron 27, 219–225.

Garcia, M.F., Gordon, M.N., Hutton, M., Lewis, J., McGowan, E., Dickey, C.A., Morgan, D., Arendash, G.W., 2004. The retinal degeneration (rd) gene seriously impairs spatial cognitive. Neuroreport 15, 73–77.

Gossage, K.W., Tkaczyk, T.S., Rodriguez, J.J., Barton, J.K., 2003. Texture analysis of optical coherence tomography images: feasibility for tissue classification. J. Biomed. Opt. 8, 570–575.

Guo, L., Salt, T.E., Luong, V., Wood, N., Cheung, W., Maass, A., Ferrari, G., Russo-Marie, F., Sillito, A.M., Cheetham, M.E., Moss, S.E., Fitzke, F.W., Cordeiro, M.F., 2007. Targeting amyloid-beta in glaucoma treatment. Proc. Natl. Acad. Sci. U. S. A. 104, 13444–13449.

Gutierrez, H., Davies, A.M., 2007. A fast and accurate procedure for deriving the Sholl profile in quantitative studies of neuronal morphology. J. Neurosci. Methods 163, 24–30.

Hsiao, K., Chapman, P., Nilsen, S., Eckman, C., Harigaya, Y., Younkin, S., Yang, F., Cole, G., 1996. Correlative memory deficits, Abeta elevation, and amyloid plaques in transgenic mice. Science 274, 99–102.

Jakobs, T.C., Libby, R.T., Ben, Y., John, S.W., Masland, R.H., 2005. Retinal ganglion cell degeneration is topological but not cell type specific in DBA/2J mice. J. Cell Biol. 171, 313–325.

Jimenez, A.J., Garcia-Fernandez, J.M., Gonzalez, B., Foster, R.G., 1996. The spatio-temporal pattern of photoreceptor degeneration in the aged rd/rd mouse. Cell Tissue Res. 284, 193–202.

Jindahra, P., Hedges, T.R., Mendoza-Santiesteban, C.E., Plant, G.T., 2010. Optical coherence tomography of the retina: applications in neurology. Curr. Opin. Neurol. 23, 16–23.

Kajic, V., Povazay, B., Hermann, B., Hofer, B., Marshall, D., Rosin, P.L., Drexler, W., 2010. Robust segmentation of intraretinal layers in the normal human fovea using a novel statistical model based on texture and shape analysis. Opt. Express 18, 14730–14744.

Klunk, W.E., Engler, H., Nordberg, A., Wang, Y., Blomqvist, G., Holt, D.P., Bergstrom, M., Savitcheva, I., Huang, G.F., Estrada, S., Ausen, B., Debnath, M.L., Barletta, J., Price, J.C., Sandell, J., Lopresti, B.J., Wall, A., Koivisto, P., Antoni, G., Mathis, C.A., Langstrom, B., 2004. Imaging brain amyloid in Alzheimer's disease with Pittsburgh Compound-B. Ann. Neurol. 55, 306–319.

Kong, J.-H., Fish, D.R., Rockhill, R.L., Masland, R.H., 2005. Diversity of ganglion cells in the mouse retina: unsupervised morphological classification and its limits. J. Comp. Neurol. 489, 293–310.

Koronyo, Y., Salumbides, B.C., Black, K.L., Koronyo-Hamaoui, M., 2012. Alzheimer's disease in the retina: imaging retinal aß plaques for early diagnosis and therapy assessment. Neurodegener. Dis. 10, 285–293.

Koronyo-Hamaoui, M., Koronyo, Y., Ljubimov, A.V., Miller, C.A., Ko, M.K., Black, K.L., Schwartz, M., Farkas, D.L., 2011. Identification of amyloid plaques in retinas from Alzheimer's patients and noninvasive in vivo optical imaging of retinal plaques in a mouse model. Neuroimage 54, S204–S217.

Lee, V., Rekhi, E., Hoh Kam, J., Jeffery, G., 2012. Vitamin D rejuvenates aging eyes by reducing inflammation, clearing amyloid beta. Neurobiol. Aging 33, 2382–2389.

Liu, B., Rasool, S., Yang, Z., Glabe, C.G., Schreiber, S.S., Ge, J., Tan, Z., 2009. Amyloid-peptide vaccinations reduce {beta}-amyloid plaques but exacerbate. Am. J. Pathol. 175, 2099–2110.

Liu, S., Li, Z.W., Weinreb, R.N., Xu, G., Lindsey, J.D., Ye, C., Yung, W.H., Pang, C.P., Lam, D.S., Leung, C.K., 2012. Tracking retinal microgliosis in models of retinal ganglion cell damage. Invest. Ophthalmol. Vis. Sci. 53, 6254–6262.

Lu, Y., Li, Z., Zhang, X., Ming, B., Jia, J., Wang, R., Ma, D., 2010. Retinal nerve fiber layer structure abnormalities in early Alzheimer's disease: evidence in optical coherence tomography. Neurosci. Lett. 480, 69–72.

Manczak, M., Calkins, M.J., Reddy, P.H., 2011. Impaired mitochondrial dynamics and abnormal interaction of amyloid beta with. Hum. Mol. Genet. 20, 2495–2509.

McEvoy, L.K., Brewer, J.B., 2010. Quantitative structural MRI for early detection of Alzheimer's disease. Expert Rev. Neurother. 10, 1675–1688.

McKinnon, S.J., Lehman, D.M., Kerrigan-Baumrind, L.A., Merges, C.A., Pease, M.E., Kerrigan, D.F., Ransom, N.L., Tahzib, N.G., Reitsamer, H.A., Levkovitch-Verbin, H., Quigley, H.A., Zack, D.J., 2002. Caspase activation and amyloid precursor protein cleavage in rat ocular hypertension. Invest. Ophthalmol. Vis. Sci. 43, 1077–1087.

Miller, N., Drachman, D.A., 2006. The optic nerve: a window into diseases of the brain? Neurology 67, 1742–1743.

Morgan, J.E., Datta, A.V., Erichsen, J.T., Albon, J., Boulton, M.E., 2006. Retinal ganglion cell remodelling in experimental glaucoma. Adv. Exp. Med. Biol. 572, 397–402.

Morin, P.J., Abraham, C.R., Amaratunga, A., Johnson, R.J., Huber, G., Sandell, J.H., Fine, R.E., 1993. Amyloid precursor protein is synthesized by retinal ganglion cells, rapidly transported to the optic nerve plasma membrane and nerve terminals, and metabolized. J. Neurochem. 61, 464–473.

Naskar, R., Wissing, M., Thanos, S., 2002. Detection of early neuron degeneration and accompanying microglial responses in. Invest. Ophthalmol. Vis. Sci. 43, 2962–2968.

Ning, A., Cui, J., To, E., Ashe, K.H., Matsubara, J., 2008. Amyloid-beta deposits lead to retinal degeneration in a mouse model of Alzheimer disease. Invest. Ophthalmol. Vis. Sci. 49, 5136–5143.

O'Brien, J., Lummis, S.C.R., 2004. Biolistic and diolistic transfection: using the gene gun to deliver DNA and lipophilic dyes into mammalian cells. Methods 33, 121–125.

O'Brien, J.A., Lummis, S.C.R., 2006. Diolistic labeling of neuronal cultures and intact tissue using a hand-held gene gun. Nat. Protoc. 1, 1517–1521.

Ohno-Matsui, K., 2011. Parallel findings in age-related macular degeneration and Alzheimer's disease. Prog. Retin. Eye Res. 30, 217–238.

Osborne, N.N., 2008. Pathogenesis of ganglion "cell death" in glaucoma and neuroprotection: focus on ganglion cell axonal mitochondria. Prog. Brain Res. 173, 339–352.

Osborne, N.N., Lascaratos, G., Bron, A.J., Chidlow, G., Wood, J.P.M., 2006. A hypothesis to suggest that light is a risk factor in glaucoma and the mitochondrial optic neuropathies. Br. J. Ophthalmol. 90, 237–241.

Paquet, C., Boissonnot, M., Roger, F., Dighiero, P., Gil, R., Hugon, J., 2007. Abnormal retinal thickness in patients with mild cognitive impairment and Alzheimer's disease. Neurosci. Lett. 420, 97–99.

Perez, S.E., Lumayag, S., Kovacs, B., Mufson, E.J., Xu, S., 2009. Beta-amyloid deposition and functional impairment in the retina of the. Invest. Ophthalmol. Vis. Sci. 50, 793–800.

Povazay, B., Hofer, B., Torti, C., Hermann, B., Tumlinson, A.R., Esmaeelpour, M., Egan, C.A., Bird, A.C., Drexler, W., 2009. Impact of enhanced resolution, speed and penetration on three-dimensional retinal optical coherence tomography. Opt. Express 17, 4134–4150.

Reynolds, E.S., 1963. Use of lead citrate at high ph as an electron-opaque stain in electron microscopy. J. Cell Biol. 17, 208–212.

Rowe, C.C., Ackermann, U., Browne, W., Mulligan, R., Pike, K.L., O'Keefe, G., Tochon-Danguy, H., Chan, G., Berlangieri, S.U., Jones, G., Dickinson-Rowe, K.L., Kung, H.P., Zhang, W., Kung, M.P., Skovronsky, D., Dyrks, T., Holl, G., Krause, S., Friebe, M., Lehman, L., Lindemann, S., Dinkelborg, L.M., Masters, C.L., Villemagne, V.L., 2008. Imaging of amyloid beta in Alzheimer's disease with 18F-BAY94-9172, a novel PET tracer: proof of mechanism. Lancet Neurol. 7, 129–135.

Rowe, C.C., Ng, S., Ackermann, U., Gong, S.J., Pike, K., Savage, G., Cowie, T.F., Dickinson, K.L., Maruff, P., Darby, D., Smith, C., Woodward, M., Merory, J., Tochon-Danguy, H., O'Keefe, G., Klunk, W.E., Mathis, C.A., Price, J.C., Masters, C.L., Villemagne, V.L., 2007. Imaging beta-amyloid burden in aging and dementia. Neurol. 68, 1718–1725.

Scheff, S.W., Price, D.A., 2003. Synaptic pathology in Alzheimer's disease: a review of ultrastructural studies. Neurobiol. Aging 24, 1029–1046.

Scheff, S.W., Price, D.A., Schmitt, F.A., Mufson, E.J., 2006. Hippocampal synaptic loss in early Alzheimer's disease and mild cognitive impairment. Neurobiol. Aging 27, 1372–1384.

Selkoe, D.J., 2002. Alzheimer's disease is a synaptic failure. Science 298, 789–791.

Smith, D.L., Pozueta, J., Gong, B., Arancio, O., Shelanski, M., 2009. Reversal of long-term dendritic spine alterations in Alzheimer disease models. Proc. Natl. Acad. Sci. U. S. A. 106, 16877–16882.

Sun, W., Li, N., He, S., 2002. Large-scale morphological survey of mouse retinal ganglion cells. J. Comp. Neurol. 451, 115–126.

Torti, C., Povazay, B., Hofer, B., Unterhuber, A., Carroll, J., Ahnelt, P.K., Drexler, W., 2009. Adaptive optics optical coherence tomography at 120,000 depth scans for non-invasive cellular phenotyping of the living human retina. Opt. Express 17, 19382–19400.

Wang, L., Dong, J., Cull, G., Fortune, B., Cioffi, G.A., 2003. Varicosities of intraretinal ganglion cell axons in human and nonhuman primates. Invest. Ophthalmol. Vis. Sci. 44, 2–9.

Wang, X., Su, B., Lee, H.G., Li, X., Perry, G., Smith, M.A., Zhu, X., 2009. Impaired balance of mitochondrial fission and fusion in Alzheimer's disease. J. Neurosci. 29, 9090–9103.

Wang, X., Su, B., Siedlak, S.L., Moreira, P.I., Fujioka, H., Wang, Y., Casadesus, G., Zhu, X., 2008. Amyloid-beta overproduction causes abnormal mitochondrial dynamics via differential modulation of mitochondrial fission/fusion proteins. Proc. Natl. Acad. Sci. U. S. A. 105, 19318–19323.

Weber, A.J., Kaufman, P.L., Hubbard, W.C., 1998. Morphology of single ganglion cells in the glaucomatous primate retina. Invest. Ophthalmol. Vis. Sci. 39, 2304–2320.

Williams, P.A., Morgan, J.E., Votruba, M., 2010. Opa1 deficiency in a mouse model of dominant optic atrophy leads to retinal ganglion cell dendropathy. Brain 133, 2942–2951.

Williams, P.A., Piechota, M., von Ruhland, C., Taylor, E., Morgan, J.E., Votruba, M., 2012. Opa1 is essential for retinal ganglion cell synaptic architecture and connectivity. Brain 135, 493–505.

Yu, D., Corbett, B., Yan, Y., Zhang, G.X., Reinhart, P., Cho, S.J., Chin, J., 2012. Early cerebrovascular inflammation in a transgenic mouse model of Alzheimer's. Neurobiol. Aging 33, 2942–2947.